Ocean Engineering 266 (2022) 113049

Contents lists available at ScienceDirect

Ocean Engineering

journal homepage: www.elsevier.com/locate/oceaneng

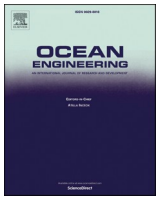

Experimental study of mooring forces on the multi-float WEC M4 in large waves with buoy and elastic cables

Peter Stansby [a,*], Sam Draycott [a], Gangqiang Li [a], Chenyu Zhao [b], Efrain Carpintero Moreno [c], Ajit Pillai [b], Lars Johanning [b]

[a] School of Engineering, University of Manchester, UK
[b] College of Engineering, Mathematics and Physical Sciences, University of Exeter, UK
[c] Department of Civil Engineering, Ghent University, 9000, Ghent, Belgium

ARTICLE INFO

Keywords:
Wave energy conversion
Articulated multi-float system
Elastic moorings
Extreme waves
Snap loads

ABSTRACT

Experiments have been undertaken in a wave basin with the hinged attenuator-type wave energy converter M4 in a 6-float configuration with two hinges for power take off (PTO), moored to a single-point buoy. This follows previous experiments with inelastic cables giving very high snap loads. The PTO was disengaged for these tests. The aims are i) to use the elastic mooring cable to reduce the snap loads of the M4 system, with two elastic stiffnesses tested, and ii) to study the system's dynamic response with a basic mooring configuration under intermediate to large waves. Mooring loads at the fairlead and the bed, and relative pitch angle between floats were measured. Numerical simulations using two different models were carried out, and the results were compared against the experiment results. For very large waves, the floats showed occasional deck submergence (dunking) limiting relative angular motion as wave height increases, in effect providing a passive end stop. The largest peak relative angle was just less than 40°. The extreme snap loads were up to 1/6th of those with inelastic cables. Spectral analyses of relative pitch angle and mooring force were made and shown to be quite different and complex.

1. Introduction

Wave energy globally has potential average power slightly less than wind (Gunn and Stock-Williams, 2012), but this has been unexploited to date. We are concerned here with wave energy converters (WECs) offshore, before the energy resource is reduced by shallow-water effects. Individual WEC capacity has been considered to be much smaller than for wind turbines and the cost of energy (COE) considerably larger. However, with multi-mode, multi-float systems, capacity may be similar to or greater than wind in some locations and COE has been estimated to be similar to offshore wind (Carpintero Moreno and Stansby, 2019; Stansby et al., 2017), and this will be improved with PTO control (Liao et al., 2021). However, survivability in extreme waves needs to be established, along with the reliability of components (Paduano et al., 2020).

The mooring is arguably the most vulnerable structural component of an offshore WEC. Snap loads are a particular problem for ultimate limit state in extreme waves while generally affecting fatigue. There is a widespread consensus in the wave energy community that mooring system design and modelling is a major challenge that needs to be overcome (Paduano et al., 2020). Design, optimization, and assessment of mooring systems require efficient hydrodynamic and dynamic mooring models, which should be fully coupled to represent all interactions. Although literature and design guidelines for conventional ocean engineering applications are abundant, they generally do not account for the requirements of wave energy conversion, where the mooring should not inhibit platform motion causing the energy generation (Davidson and Ringwood, 2017; Johanning and Smith, 2009; Paduano et al., 2020; Thomsen et al., 2018). Wave basin testing, which is both controlled and relatively inexpensive, is desirable for basic understanding and validation of models prior to ocean deployment.

There are various mooring options: catenary slack moored, elastic taut moored, combinations with single point (buoy) moorings (Davidson and Ringwood, 2017), and elastic nylon/polyester ropes offer an economical option (Weller et al., 2015), while reducing snap loads (Paduano et al., 2020). Some of these options have been assessed for

* Corresponding author.
E-mail address: p.k.stansby@manchester.ac.uk (P. Stansby).

https://doi.org/10.1016/j.oceaneng.2022.113049
Received 8 June 2022; Received in revised form 14 October 2022; Accepted 28 October 2022
Available online 9 November 2022

floating wind platforms (Xu et al., 2021).

There are some experimental data for a single buoy on a taut elastic cable (Hann et al., 2018) and for the hinged attenuator-type 6-float wave energy converter M4 with a single point mooring in uni-directional waves with inelastic cables (Stansby and Carpintero Moreno, 2020a). An important observation for M4 is that in large waves, as well as small-to-intermediate waves, the pitch response is almost linear (Santo et al., 2017), while the mean mooring force is highly nonlinear, and snap loads can be massive with inelastic cables (Stansby and Carpintero Moreno, 2020b). A preliminary numerical model investigation suggested that snap loads may be almost eliminated with elastic cables when combined with a single-point buoy (Stansby and Carpintero Moreno, 2020b).

However there has been no experimental testing of multi-float WEC configurations to assess the efficacy of elastic cables in reducing snap loads to the authors' knowledge. For this paper, wave basin experiments were undertaken for the 6-float M4 with a single elastic mooring line connected to the mooring buoy, and hawser from buoy to bow float. This may be considered the most basic configuration investigated previously. Large irregular waves are investigated, larger than previously with an inelastic cable, up to the breaking limit. The PTO was disengaged for these tests. Comparisons will be made with the industry standard Orcaflex code, and an in-house linear diffraction-radiation code M4hydro with mean forces included (Stansby and Carpintero Moreno, 2020a, b). The principal aim of the paper is to study M4 system dynamics with an elastic mooring cable under intermediate to large waves. A single mooring configuration with two different elastic stiffnesses is considered and tested.

The paper is organised as follows. The experimental arrangement, including the WEC configuration, the mooring configuration, the wave basin and wave conditions, the elastic mooring cables, and the measurements to be made, will be described in the next section. The following section 3 shows some video snapshots of multi-float/buoy motion in extreme waves, results for the mooring forces and pitch angles, with some spectral analysis. Comparisons are made with the Orcaflex model and the in-house M4hydro model in section 4. The forces for a full-scale system at Wavehub, assessed to be 50x model scale, are determined for a scatter diagram in section 5, based on Froude scaling. Results are discussed in section 6, including previous inelastic cable results. Overall conclusions are drawn in section 7.

2. Experimental arrangement

2.1. WEC configuration

As shown in Fig. 1, the 6-float version of M4 consists of a bow float and three mid floats, effectively forming a rigid body, and two stern floats with beams hinged above the outer mid floats as used in (Carpintero Moreno and Stansby, 2019). The wave forces on individual floats are due to heave, surge and pitch to a lesser degree, resulting in pitch motion about the hinge points (Stansby et al., 2015). The system heads naturally into the wave direction due to drift forces and with the uni-directional waves used here the pitch motions at each hinge are almost identical. The dimensions in plan view are shown in Fig. 2(a) and elevation view in Fig. 2(b).

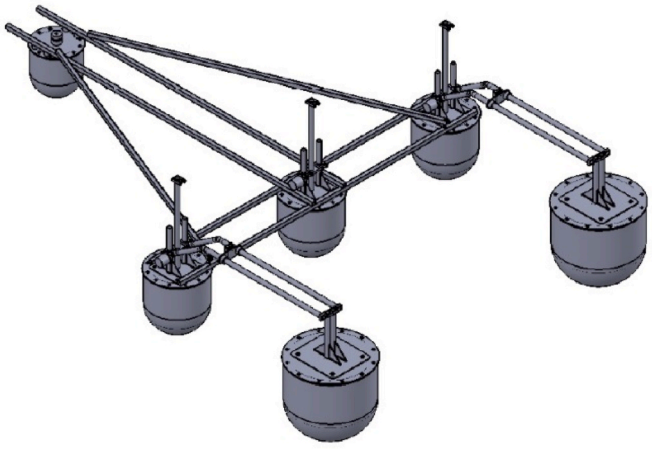

Fig. 1. Isometric view of M4 6-float WEC system.

The masses and inertias for the device are given in Table 1.

The natural frequencies will also be of interest. For individual floats in heave, these are 1.35 Hz for the bow and mid floats and 0.95 Hz for the stern float, taking account of added mass. There is no surge natural frequency for individual floats. There are natural frequencies associated with the beam lengths as there will be resonance when the forces on the bow and mid floats are in anti-phase and when the mid and stern floats are in anti-phase. This corresponds with beam lengths of 1.33 m and 0.8 m being half a wavelength given by wave frequencies of 0.76 Hz and 0.99 Hz based on linear dispersion. These will be referred to as pitch natural frequencies. A range of natural frequencies is intended to give broadband response for wave energy conversion although this is not considered here.

2.2. Mooring configuration

The mooring to the bow float is shown in Fig. 3, comprising an elastic cable from the bed to a spherical buoy and an almost inelastic cable from the buoy to the fairlead on the bow float. The buoy weighs 87 g with a diameter of 110 mm.

2.3. Wave basin

The experiments were undertaken in the Lir Ocean Basin of University College, Cork, Ireland, with a curved line of 80 wave makers with sloping beaches on two sides, as shown in Fig. 4 with dimensions. Fig. 5 shows an aerial photo of the configuration in the basin with a mooring system, including the mooring line and buoy.

The wave direction is at 63° relative to the normal of the long beach so that wave reflection generally occurs from two beaches before returning to the working area and is considered to be less than 10% (Carpintero Moreno and Stansby, 2019). The device aligns naturally with the wave direction due to drift forces. Wave conditions (surface elevations) were measured by wave probes without the device in place and also by wave probes alongside the device. The runs were 10 min long representing about 1-h full scale at 1:50 scale (based on Froude scaling). Wave conditions are listed in Table 2 for the chosen T_p values (1.0, 1.2, 1.4, 1.8 s) with spectral peakedness factor $\gamma = 3.3$, which is widely used as standard for JONSWAP spectra defining fetch-limited waves (Hasselmann, 1973). γ values of 1 and 2 were also investigated but are not presented here. The target H_s were 0.06, 0.09, 0.13 and 0.16 m with larger values representing the limit of the wave basin capability. These correspond to full-scale values of T_p (7.1, 8.5, 9.9, 12.7 s) and H_s (3, 4.5, 6.5, 8 m) covering the range for typical sites, e.g. Wavehub in section 5.

The actual H_s were determined from 4σ, where σ is the standard deviation of the measured surface elevation, listed in Table 2 with the resulting root mean square error (RMSE) error to the JONSWAP spectral fit, normalised by σ. The target H_s for the spectra were generally underestimated, up to 5% for smaller values and 11% for the large values, where breaking dissipates some wave energy. With $T_p = 1$ s, the largest possible H_s was 0.081 m and 0.116 m with $T_p = 1.2$s, both with occasional breaking, associated with a spectral wave steepness $H_s/L_p = 0.052$, given in Table 2. The slightly lower value of 0.046 for $T_p = 1.4$s also gave occasional breaking. Example spectra are shown for the largest H_s with $T_p = 1.2$, 1.4, and 1.8 s in Fig. 6. The measured spectral peak is greater than the JONSWAP fit at close to maximum steepness with $T_p =$

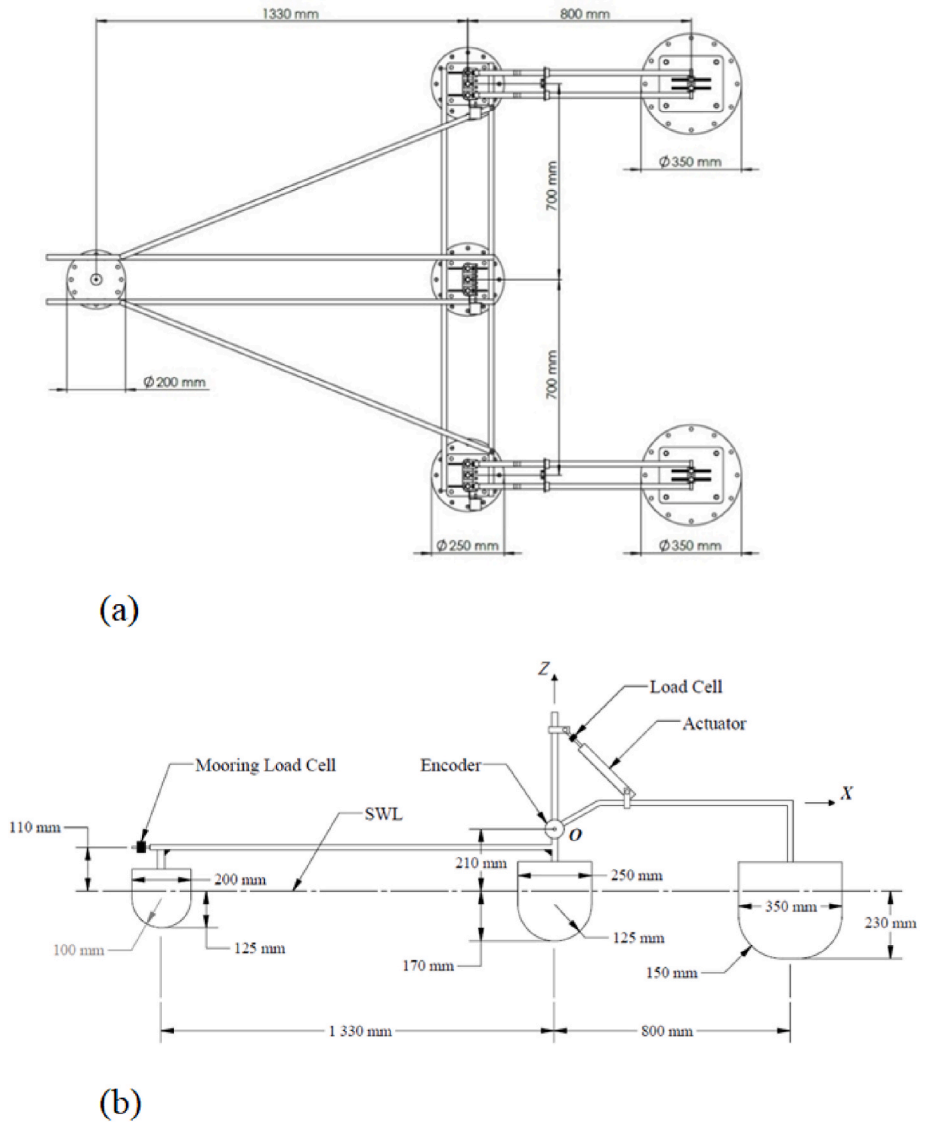

Fig. 2. (a) Plan of M4 system with dimensions, (b) elevation of M4 system with dimensions, note freeboard is 100 mm for all floats.

Table 1
Mass of each component with centre of mass position and inertia relative to hinge O.

	Mass (*kg*)	x_g (*m*)	y_g (*m*)	z_g (*m*)	I_{yy} $kg.m^2$)
Bow float	1.465	−1.356	0	−0.181	2.761
Bow/mid beams	2.467	−0.456	0	−0.071	1.069
Mid float port	2.845	−0.026	0.705	−0.160	0.132
Ballast	2.700	−0.027	0.710	−0.321	0.288
Mid float centre	2.845	−0.026	0.005	−0.160	0.132
Ballast	2.700	−0.027	0	−0.321	0.288
Mid float right	2.845	−0.026	−0.694	−0.160	0.132
Ballast	2.700	−0.027	−0.699	−0.321	0.288
Beams mid/stern	0.525	0.328	±0.697	0.087	0.090
Stern float	4.041	0.772	±0.700	−0.204	2.680
Ballast	13.000	0.772	±0.700	−0.350	9.438

1.2 s and 1.4 s while the peaks are almost coincident with the smaller steepness of 0.029 for $T_p = 1.8$ s. The normalised RMSE was always less than 12%.

2.4. Elastic cable characteristics

The cables used were elastic Bungee cords of 8 mm and 10 mm in diameter (made from rubber and polyester, Greenpromise, 2021) which are almost neutrally buoyant, with an effective density of less than about 1% that of water. As shown in Fig. 3, the unstretched length to the buoy was 1.27 m. The static elastic behaviour was determined by measuring extension due to hanging weights in 1 kg increments to one end, and variations are shown in Fig. 7. The 8 mm diameter cord is referred to as E2 and 10 mm as E3. A smaller diameter of 6 mm (E1) gave device movement just outside the working area and was not used. The form of the curves is closely parabolic. The process was repeated daily during testing. Results for the more elastic case E2 (smaller diameter), which gave smaller mooring forces of most interest, are presented mainly. The mooring buoy also has effective static stiffness as the float position determines the mooring force dependent on the buoyant force on the buoy. This is added to the elastic behaviour of the more elastic case E2 and shown in Fig. 7, although not used directly in a mooring model. The Bungee cords have relatively low elasticity for the small force, which increases as force increases while the effective elasticity due to the buoy is the opposite: high for small force becoming low, eventually inelastic, as force increases. The combined effect is more closely linear.

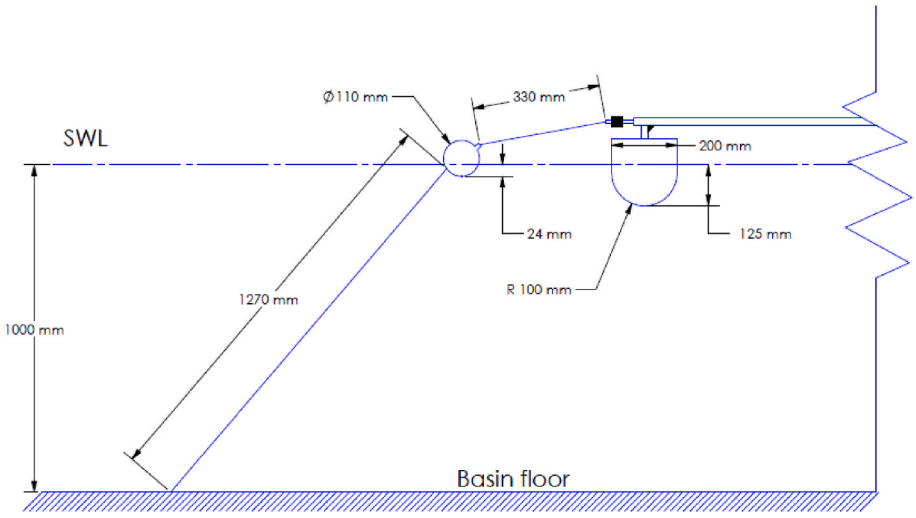

Fig. 3. Mooring configuration of the physical experiment showing the buoy and bow float; the 1.27 m mooring line is elastic, with characteristics defined in Fig. 7, and the 0.33 m hawser effectively inelastic.

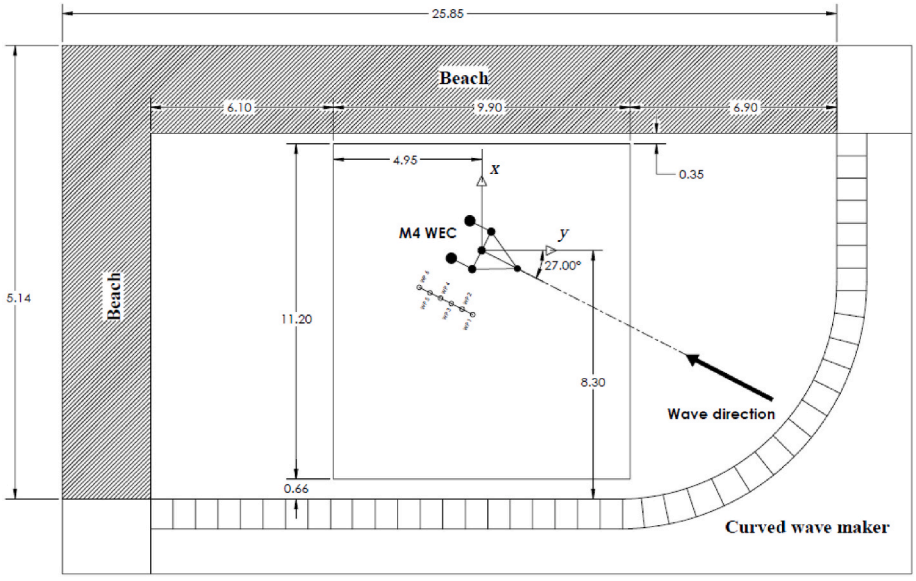

Fig. 4. Lir Ocean Basin of University College, Cork, showing wavemakers, beach and M4 WEC, with dimensions in m.

Fig. 5. Aerial photo of WEC with mooring in the wave basin.

2.5. Measurements made

The following measurements were made over the 10 min wave duration. (i) Longitudinal mooring force on the bow float (using 100 N load cell with 0.15% accuracy from Omega Engineering Inc.). (ii) Force on the mooring line attached to the bed (using submersible 445 N load cell with 0.02% accuracy from FUTEK Advanced Sensor Technology Inc.). (iii) Qualisys measurement of the position of each float from reflective spheres above each float. This gives the angular rotation between the bow/mid floats and the stern floats. The sampling rate for (i) was 200 Hz (with imported data acquisition) and for (ii) and (iii) was 50 Hz (in house data acquisition).

Table 2
Values of H_s and normalised RMSE for different T_p values.

T_p (s)	L_p (m)	H_s (m) target				max spectral steepness H_s/L_p
		0.06	0.09	0.13	0.16	
		measured $H_s = 4\sigma$ (RMSE normalised with σ)				
1.0	1.56	0.057 (9.9%)	0.081 (11.7%)	–	–	0.052
1.2	2.25	0.059 (7.7%)	0.087 (8.0%)	0.116 (10.0%)	–	0.052
1.4	3.05	0.057 (9.9%)	0.086 (9.6%)	0.119 (9.0%)	0.142 (8.9%)	0.046
1.8	5.00	0.056 (10.3%)	0.083 (9.5%)	0.119 (9.0%)	0.145 (8.8%)	0.029

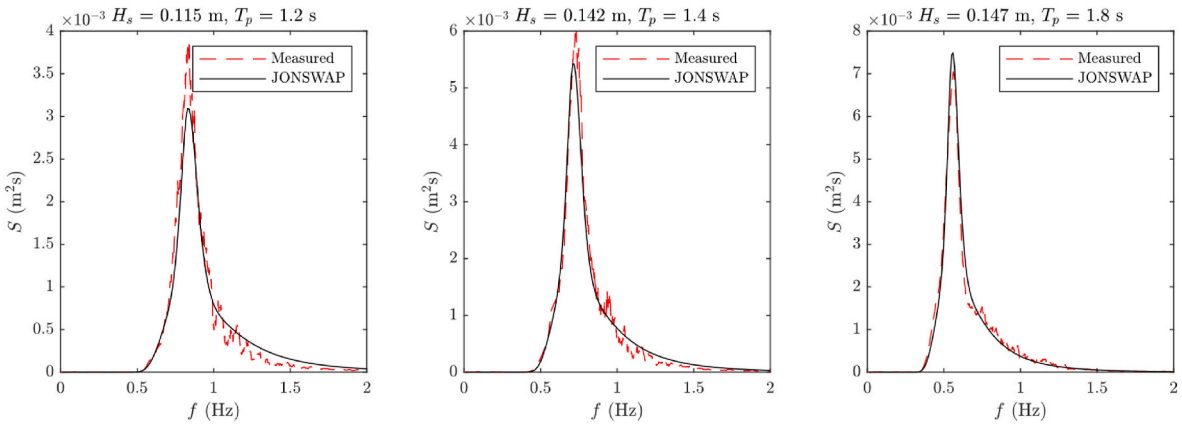

Fig. 6. Spectra for largest wave cases with JONSWAP fit based on measured H_s.

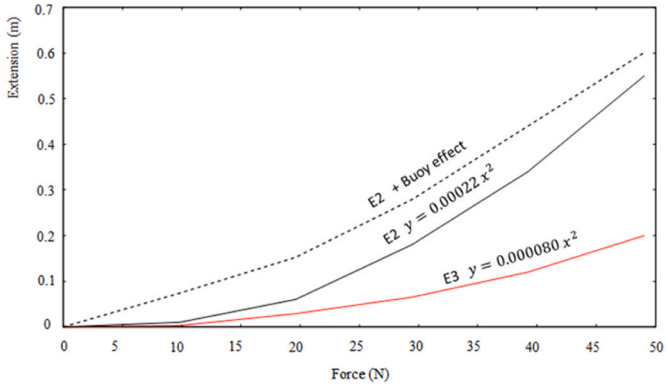

Fig. 7. Extension versus force characteristics for the Bungee cords. E2 is bungee cord with 8 mm diameter and E3 has 10 mm diameter.

3. Experimental results

Wave conditions were listed in Table 2. Some video snapshots with the WEC are shown in Figs. 8–10 for T_p = 1.2 and 1.4 s with breaking waves, and 1.8 s. The red mooring buoy is occasionally fully submerged (not visible), and the extreme motion of the floats is apparent, with all floats being submerged at some time. Overtopping the deck generates splashing and dissipation of energy as well as a downward force.

Example time series for surface elevation, relative angles, fairlead (top) and bed mooring forces are shown in Fig. 11 for the case with H_s = 0.142 m and T_p = 1.4 s, shown in Fig. 9, which gives the largest forces. The time interval 426–448 s covers some peak forces and demonstrates the complexity of interaction between wave profile, angular response and forces.

The mean and peak longitudinal fairlead forces for all cases are shown in Fig. 12 for the more elastic case (E2) and Fig. 13 for the less elastic case (E3). It is apparent that the peak forces reach a maximum as H_s increases and are similar for $T_p \leq 1.4$ s, where spectral wave steepnesses are close to limiting. For T_p = 1.8s larger H_s and hence greater steepness would be needed to generate a similar peak force but this was not possible in the wave basin. The mean forces are largest for T_p = 1.2 s and 1.4 s which are close to pitch resonance at 1.31 s for the bow/mid floats. There is a small residual mean force due to the electrical cable connection from the device to the gantry; this is approximately 1 N. This is subtracted from the measured force to give the mooring force and any negative value set to zero. While this is justified on a quasi-steady basis the small residual force may affect the dynamics for smaller H_s when the mean mooring force is of similar magnitude. The emphasis of this study is on extreme waves, and results for smaller waves are also included.

All further results use the more elastic cable (E2) with the smaller mooring forces, which are of the most interest. The small cable diameter in relation to other dimensions, e.g. buoy diameter, was considered to have negligible effect and this was supported in Orcaflex runs. The mean fairlead and bed tension forces are shown in Fig. 14 and the peak forces

Fig. 8. Snapshots from video for H_s = 0.116 m and T_p = 1.2 s.

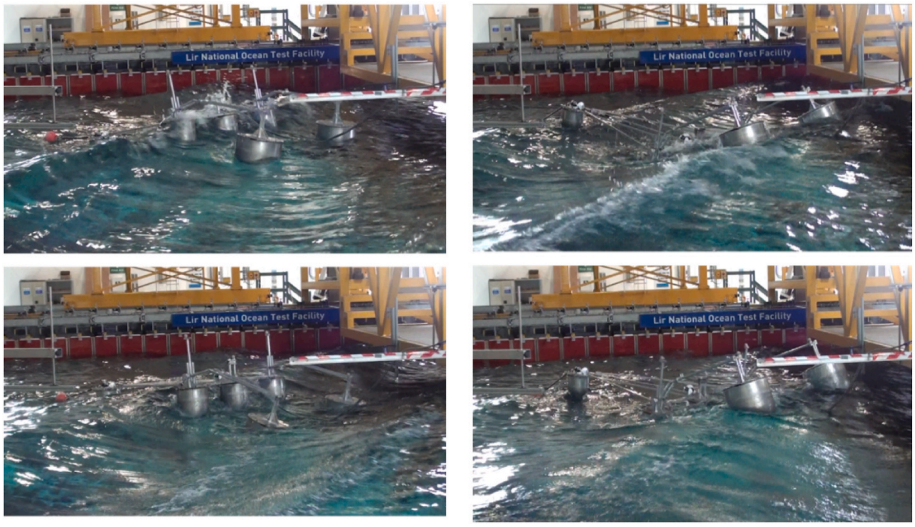

Fig. 9. Snapshots from video for $H_s = 0.142$ m and $T_p = 1.4$ s.

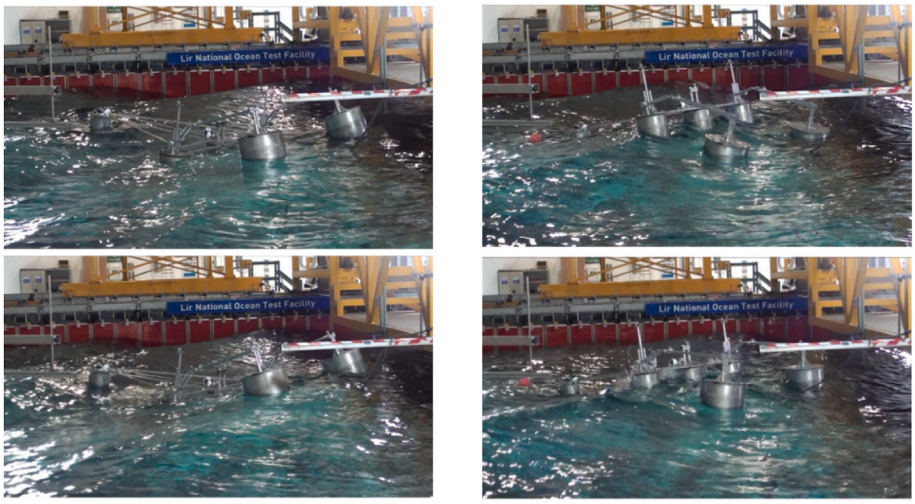

Fig. 10. Snapshots from video for $H_s = 0.145$ m and $T_p = 1.8$ s.

in Fig. 15. The fairlead forces for a given T_p are always smaller. It is apparent that the mean forces continue to increase markedly with H_s up to the maximum while the peak forces flatten out. These results are for $\gamma = 3.3$, but the same occurred with values of $\gamma = 2$ and 1.

The motion of the system is described by the relative pitch angle θ_{rel} between floats, obtained from Qualysis. Rms and peak values are shown in Fig. 16. The peak values become saturated with H_s for $T_p \leq 1.4$ s, although the values for $T_p = 1.2$ and 1.4 s are larger than for $T_p = 1$ s. The largest peak values are just less than 40°; this was also the case for the less elastic cable (E3) except for one value of 46°.

Spectra of relative angle and mooring force are now shown for wave cases with smaller and largest H_s for given T_p, as listed in Table 3. Fig. 17 shows spectra of the relative angle for the smaller H_s and Fig. 18 for the largest H_s.

It is apparent that the spectral peaks occur at the bow/mid pitch natural frequency close to 0.76 Hz, except for the case with $T_p = 1.0$ s where the peak in the spectrum coincides with the mid/stern natural pitch frequency of 0.99 Hz. Note these pitch frequencies are derived from linear dispersion and nonlinear effects will cause small differences. The same occurred with $H_s = 0.081$ m (not shown). There is a small peak at the wave frequency with $T_p = 1.8$ s and is just discernible with $T_p = 1.4$s where the response is quite broadband for the largest H_s. Spectra for bed and fairlead (top) mooring forces are shown in Fig. 19 for the smaller H_s and in Fig. 20 for the largest H_s.

The spectra for bed and top forces have a similar form as expected, and the bed magnitudes generally are larger than the top magnitudes. However, the spectra are more complex than for relative pitch angle. The mean component is apparent as frequency decreases to zero. There are prominent peaks close to the peak wave frequency, 0.99 Hz, 1.75 Hz, 2.6 Hz and 3.4 Hz to a lesser degree. 0.99 Hz is the mid/stern pitch natural frequency and peaks are not evident at the bow/mid pitch frequency of 0.76 Hz although this is similar to f_p with $T_p = 1.2$ and 1.4s but not for 1.8 s. The frequency of 1.75 Hz appears to be due to the sum of the pitch frequencies for bow/mid and mid/stern floats, possibly coinciding with a buoy/mooring natural frequency. For $T_p = 1$ s, a second harmonic peak at twice the mid/stern pitch frequency is evident but not for larger T_p. There is also a small peak at 2.6 Hz with $T_p = 1.2$ s and a smaller peak at 3.4 Hz; there is visual (video) evidence of intermittent high-frequency mooring buoy motion, although this was not measured directly. The natural frequency of a half-immersed buoy would be 2.6 Hz and the buoy position varies between no immersion and being fully immersed. The small 3.4 Hz peak is probably a structural frequency. Thus, the mooring force spectra are quite different from the angular response spectra.

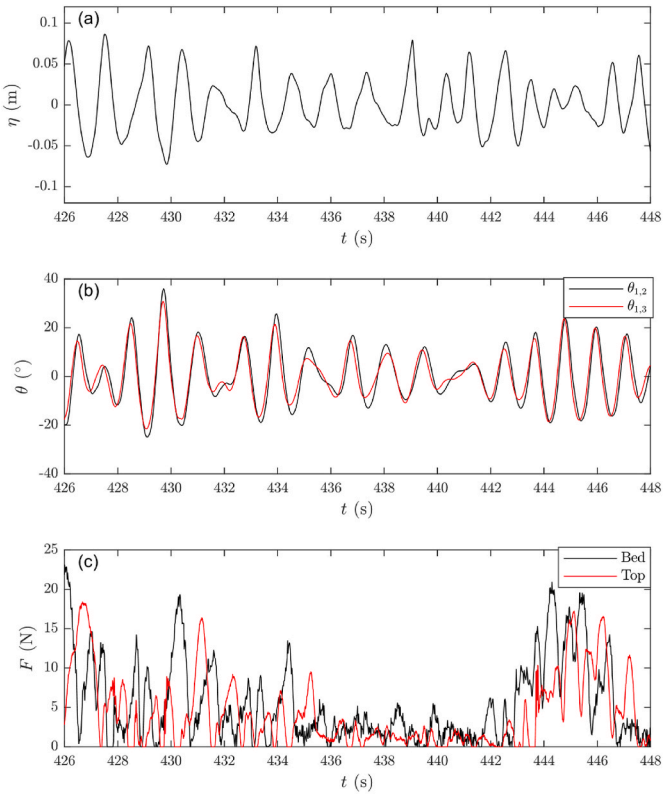

Fig. 11. Time series of (a) surface elevation (η), (b) relative angles (θ), (c) fairlead (top) and bed mooring forces (F) for the extreme case, shown in Fig. 9, with $H_s = 0.142$ m and $T_p = 1.4$ s.

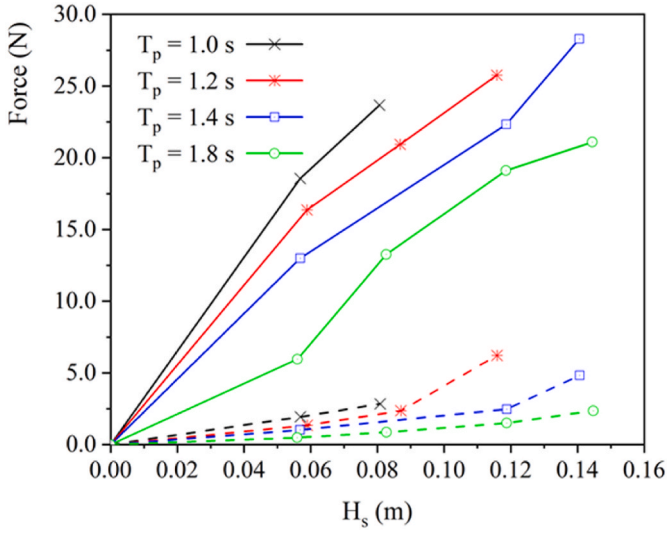

Fig. 12. Measured mean (dashed line) and peak fairlead (full line) forces for elasticity E2.

Finally, the natural frequency in surge for the overall system is important for possible low-frequency excitation due to different frequencies. The total dry mass is 55.7 kg, and surge added mass is 34.0 kg giving an equivalent mass of 89.7 kg. With a representative equivalent stiffness of 80 N/m, the natural frequency is approximately 0.19 Hz with a period of 7 s. There is certainly spectral content in the mooring forces close to this low frequency but no obvious peak indicating resonance.

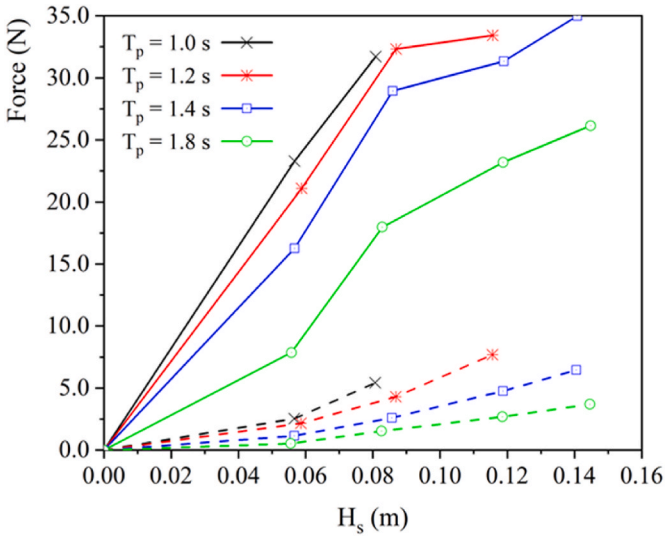

Fig. 13. Measured mean (dashed line) and peak (full line) fairlead forces for elasticity E3.

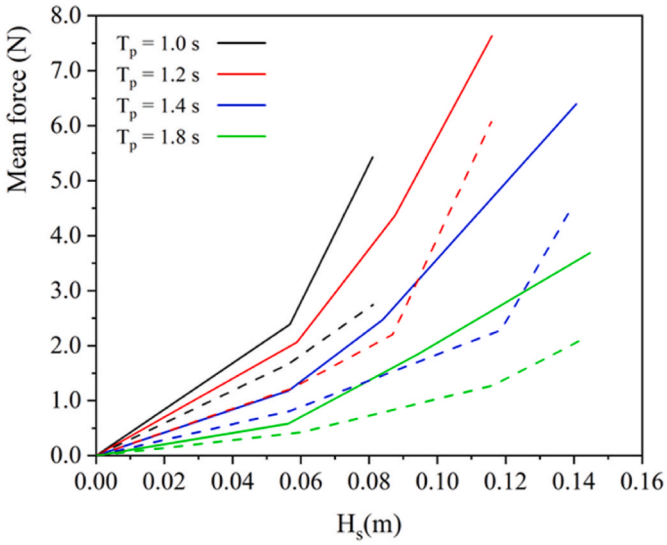

Fig. 14. Mean fairlead force (dashed line) and bed tension (full line) for elasticity E2.

4. Model results

Widely used hydrodynamic models coupled with mooring models are based on linear diffraction-radiation models in the time domain using the Cummins method (Cummins et al., 1962)). Second-order effects that give mean drift forces are added. While the wave-body interactions in this study are highly nonlinear, it is of interest to assess results from such models. Two models are considered: the industry-standard Orcaflex model (Orcaflex, 2012) with a lumped mass mooring model and an in-house model M4hydro where mean forces are determined from radiation and drag energy flux absorbed and a quasi-steady mooring (Stansby and Carpintero Moreno, 2020a, b).

Full results of Orcaflex will be presented in (Zhao et al., 2022). The model includes linear and second-order drift forces with an elastic mooring defined for E2. Time stepping is explicit with a variable time step marching scheme. Drag on floats is not included. The hawser is given a stiffness about an order of magnitude greater than the elastic cable. For cases in Table 3, errors are shown in block form in Fig. 21. The model generally underestimates relative angle and mooring forces

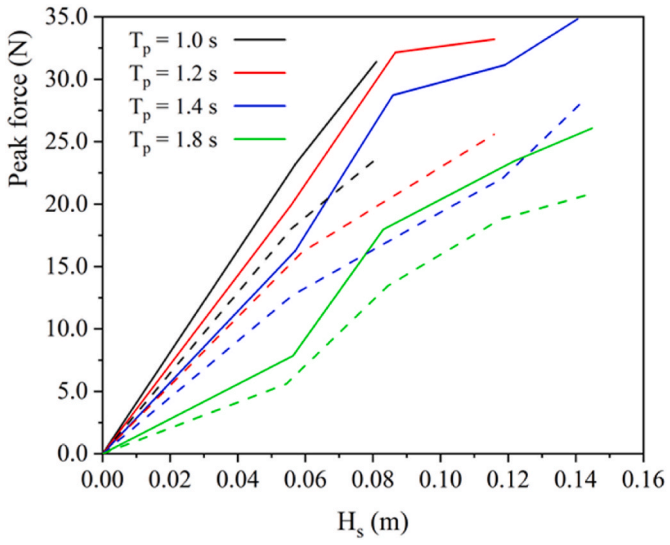

Fig. 15. Peak fairlead force (dashed line) and bed tension (full line) for elasticity E2.

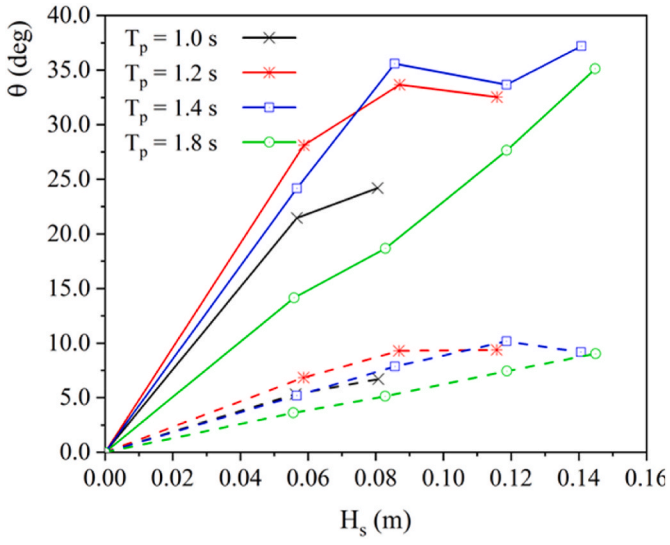

Fig. 16. Relative angle θ_{rel} (degrees) versus H_s with elasticity E2. Peak (full lines), rms (dashed lines).

Table 3
Values of largest and smaller H_s for different T_p values.

T_p (s)	1.0	1.2	1.4	1.8
Smaller H_s (m)	0.057	0.059	0.057	0.056
Largest H_s (m)		0.116	0.142	0.144

except for the peak fairlead forces, which are overestimated. The peak angular response underprediction was within 50% and peak fairlead force overestimation was within 42% for smaller waves and 110% for larger waves. Run times were approximately 15 h with an i7 processor.

For the M4hydro model, the linear Cummins model is run first with mean second-order forces for stationary floats, and hydrodynamic coefficients are obtained through WAMIT (Lee and Newman, 2013). A drag coefficient of unity is assumed for the floats to account for losses due to splashing as well as drag, tuned for the large waves. The mean power due to radiation and drag from all floats for all modes is calculated; In this case, the relevant modes are heave, surge, and pitch local to each float; pitch is a small effect. The mean force due to these damping forces is assumed to be equal to their mean power absorbed divided by the wave speed, see (Mei, 1989) for two dimensions. This formula is strictly valid for regular waves and is assumed for the narrow band waves used here using the wave speed for the peak period. The model is rerun with mean force due to damping added to the drift force for the stationary body. The dynamic response is affected negligibly by the revised mean force. This simple formulation obviously omits second-order non-zero difference and sum frequency effects which are included in Orcaflex. The mooring is assumed to be quasi-steady and only the buoyancy of the buoy assuming still water level is included. The mooring formulation given in (Stansby and Carpintero Moreno, 2020b) is precise within this context. The comparison results with the experimental data are shown in Fig. 22. The rms relative angles are overestimated by up to 24% for small waves and 36% for large waves, and peak values are underestimated by up to 29% for small waves and 25% for large waves.

The mean mooring forces are relatively small, up to about 2 N for small waves and 7 N for large waves, and generally overestimated by up to 64% for small waves and 36% for large waves. The peak values are underestimated by up to about 70% for small and large waves. Model running for 10 min in real time requires about 5 min running time on a standard laptop with an i5 processor. The model was generated mainly to investigate response and power from multiple float configurations and enable PTO control, requiring efficient real-time prediction, e.g. (Liao et al., 2021).

5. Mooring forces at Wavehub

In order to assess full scale mooring forces, a scatter diagram for a representative site Wavehub in SW UK is applied, relating to one year from February 2005 to April 2006 (Pillai et al., 2018). For a laboratory $T_p = 1.2$ s, close to pitch resonance, a scale of 1:50 gives $T_p = 8.5$ s with Froude scaling. Assuming $\gamma = 3.3$ the energy period for a JONSWAP spectrum is given by $T_e = 0.86\ T_p$, giving $T_e = 7.3$ s, close to the most likely period. The H_s/T_e scatter diagram for peak fairlead force is shown in Table 4, and for mean fairlead force in Table 5, showing % occurrence in brackets.

This suggests a maximum peak load of 312 tonnes with a mean of 50 tonnes. With a total mass for the 6-float system with a ballast of 6962 tonnes, this peak force is only 4.5% of the dry weight. The peak tension at the bed is up to 40% larger. The cables' extension-force curves in Fig. 7 give stiffness EA/l_0 of about 100 and 275 N/m for force >15 N, where E is Young's modulus, A is cross-sectional area and l_0 is unstretched length. This corresponds to 250 and 700 kN/m at full scale, which is within the design capability of synthetic cables (Thomsen et al., 2018), although this can only be an approximate linear assessment since the nonlinear Bungee cord characteristics are different from full-scale synthetic cables. However, these relatively small loads for articulated multi-floats systems with elastic moorings suggest the potential for floating offshore platforms more generally, beyond wave energy conversion.

6. Discussion

The mooring is often considered the most vulnerable structural component for a wave energy converter. For the attenuator-type moored multi-float WEC M4, a mooring line from the bed was attached to a buoy with a hawser to the bow float. In previous wave basin experiments with inelastic cables, a peak fairlead mooring force of 148 N was measured with $T_p = 1.4$ s, $H_s = 0.13$ m; 105 N with $T_p = 1$ s, $H_s = 0.074$ m; and 48 N with $T_p = 2.0$ s, $H_s = 0.082$ m (Stansby and Carpintero Moreno, 2020a). Such high snap loads are undesirable. With the elastic cords used here, the peak fairlead forces are reduced to below 30 N for the more elastic cable (E2) and below 40 N for the stiffer cable (E3); the wave heights tested were also greater, close to limiting wave steepness.

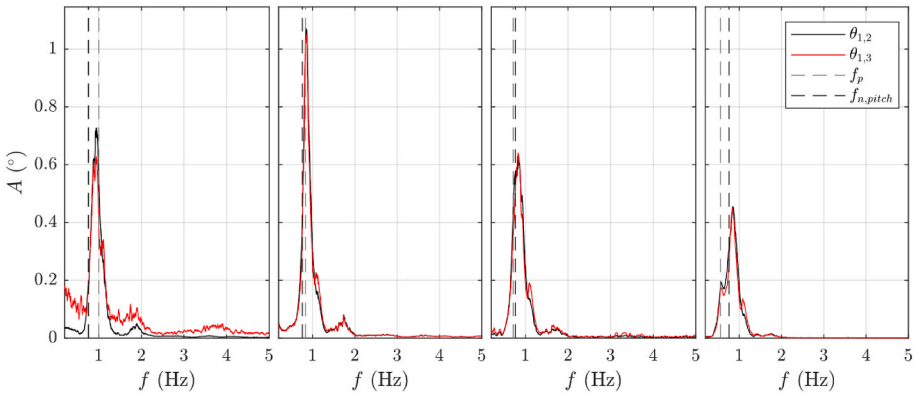

Fig. 17. Relative angle spectra at both hinges, $\theta_{1,2}$ and $\theta_{1,3}$, for smaller H_s. f_p is peak frequency and bow/mid pitch natural frequency $f_{n,pitch} = 0.76$ Hz.

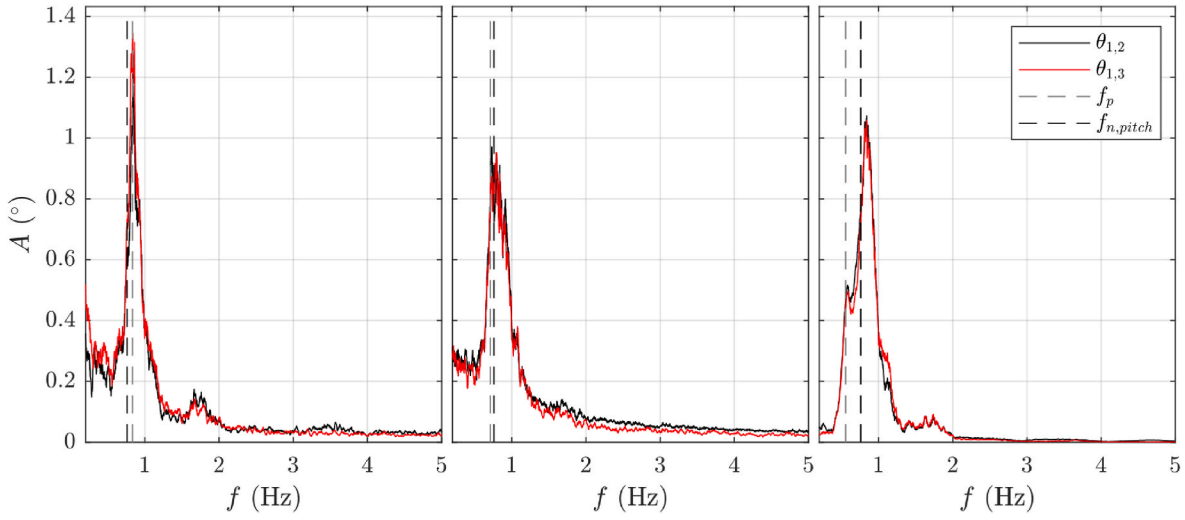

Fig. 18. Relative angle spectra at both hinges, $\theta_{1,2}$ and $\theta_{1,3}$, for largest H_s. f_p is peak frequency and bow/mid pitch natural frequency $f_{n,pitch} = 0.76$ Hz.

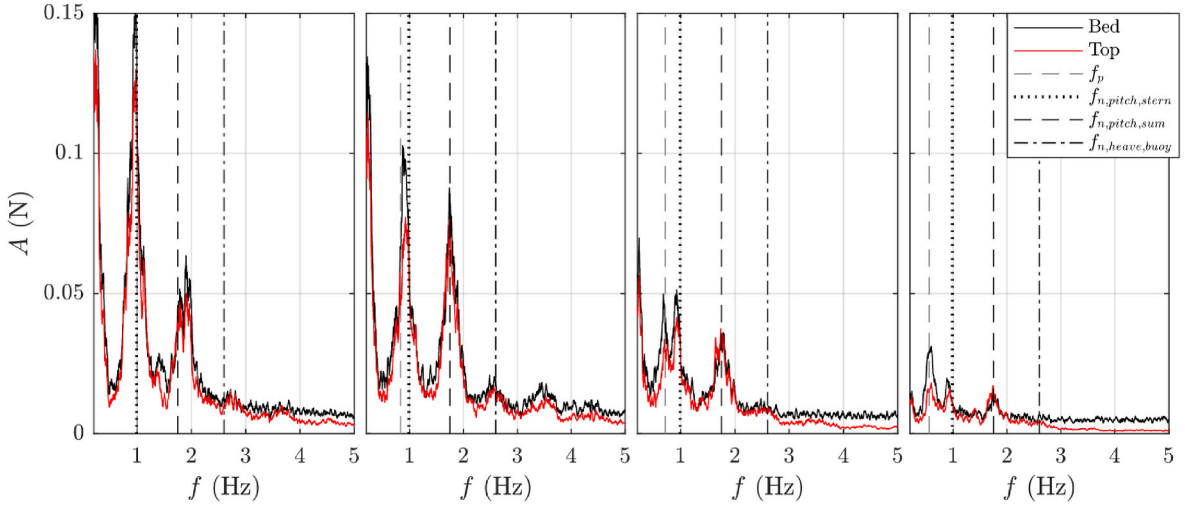

Fig. 19. Mooring force spectra, at bed and top (fairlead), for small H_s with $T_p = 1.0, 1.2, 1.4, 1.8$ s f_p is peak frequency, pitch natural frequencies are: mid/stern $f_{n,pitch,stern} = 0.99$ Hz; sum of bow/mid and mid/stern natural frequencies $f_{n,pitch,sum} = 1.75$ Hz; buoy $f_{n,heave,buoy} = 2.6$ Hz (estimated).

The hawser was effectively inelastic. Such large reductions in snap load are clearly beneficial. The increase in snap load by about 30% is associated with an increase in elastic stiffness by a factor of 2.75 (from parabolic curves shown in Fig. 7). With the inelastic cable, the maximum snap load of 148 N with $H_s = 0.13$ m and $T_p = 1.4$ s is reduced by a factor of 6–25 N with the more elastic cable, see Fig. 11.

In large, occasionally breaking waves, the motion of the floats is observed to be quite nonlinear with submergence varying considerably,

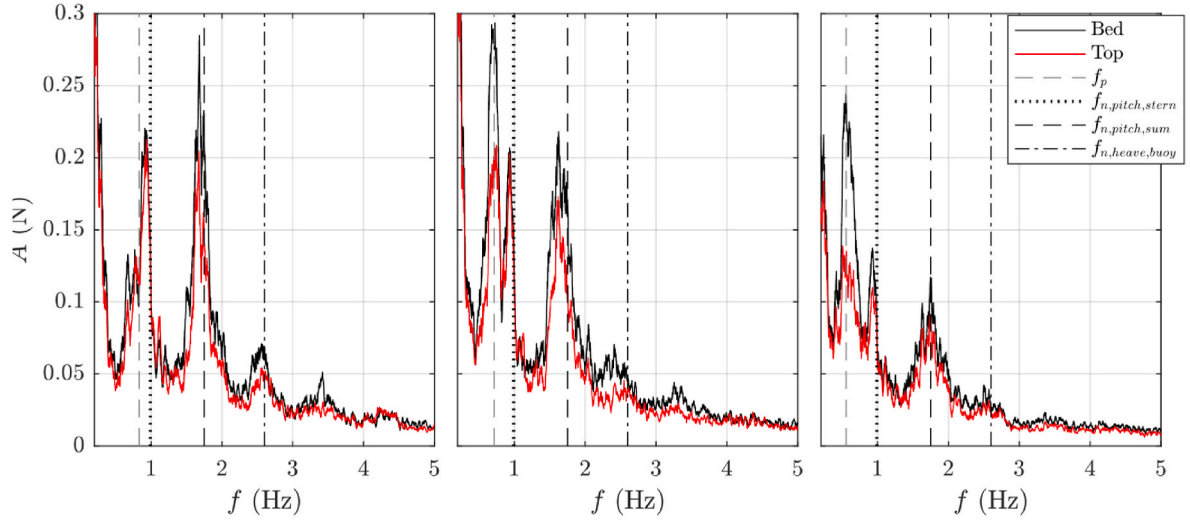

Fig. 20. Mooring force spectra, at bed and top (fairlead), for large H_s with T_p = 1.2, 1.4, 1.8 s f_p is peak frequency, pitch natural frequencies are: mid/stern $f_{n,pitch,\ stern}$ = 0.99 Hz; sum of bow/mid and mid/stern natural frequencies $f_{n,pitch,\ sum}$ = 1.75 Hz; buoy $f_{n,heave,\ buoy}$ = 2.6 Hz (estimated).

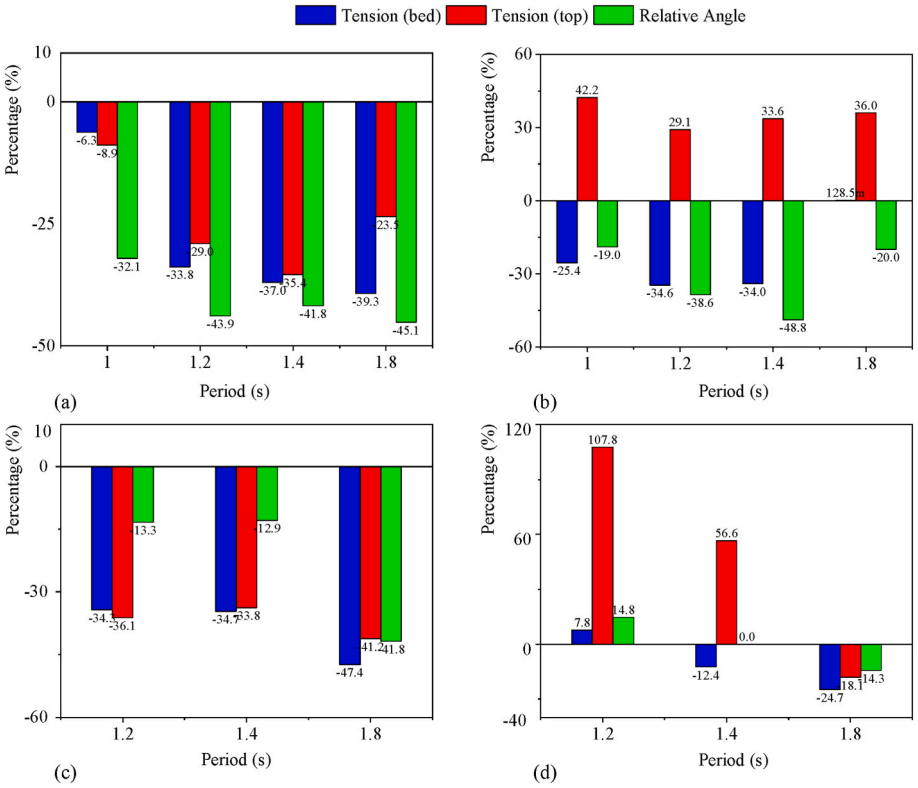

Fig. 21. Orcaflex errors in mooring forces and relative angle for cases in Table 3: (a) mean tension and rms relative angle for small H_s, (b) peak values for small H_s, (c) mean tension and rms relative angle for large H_s, (d) peak values large H_s.

from fully submerged (dunked) to almost airborne. This dunking with overtopping advantageously limits peak relative angular motion as associated with strong energy dissipation due to splashing, effectively a passive end stop. This has previously been investigated for a single float (Stallard et al., 2009). The peak relative angle becomes saturated at less than 40° for the more elastic cable. The peak forces also reach maxima as H_s is increased to limiting steepness, suggesting magnitudes that will not be exceeded, e.g. 35 N at the bed for the more elastic cable.

Froude scaling is conventionally applied to convert laboratory wave basin values to full scale, Wavehub in this case. Reynolds numbers at laboratory and full scale are generally orders of magnitude different affecting drag coefficient, but drag is likely to be relatively a small force compared to radiation damping for these rounded shapes. This has been demonstrated by validated computational fluid dynamics (CFD) for float motion in still water (Gu et al., 2018) and this is likely to be the case for these experiments. The violent overtopping of floats and splashing that occurs in large waves is gravity dominated and the resulting forces will also follow Froude scaling. Determining full-scale effects in this way is thus thought to be justified.

The models give quite approximate predictions as might be expected with small amplitude assumptions applied to a highly nonlinear problem. However, since angular response from experimental analysis of

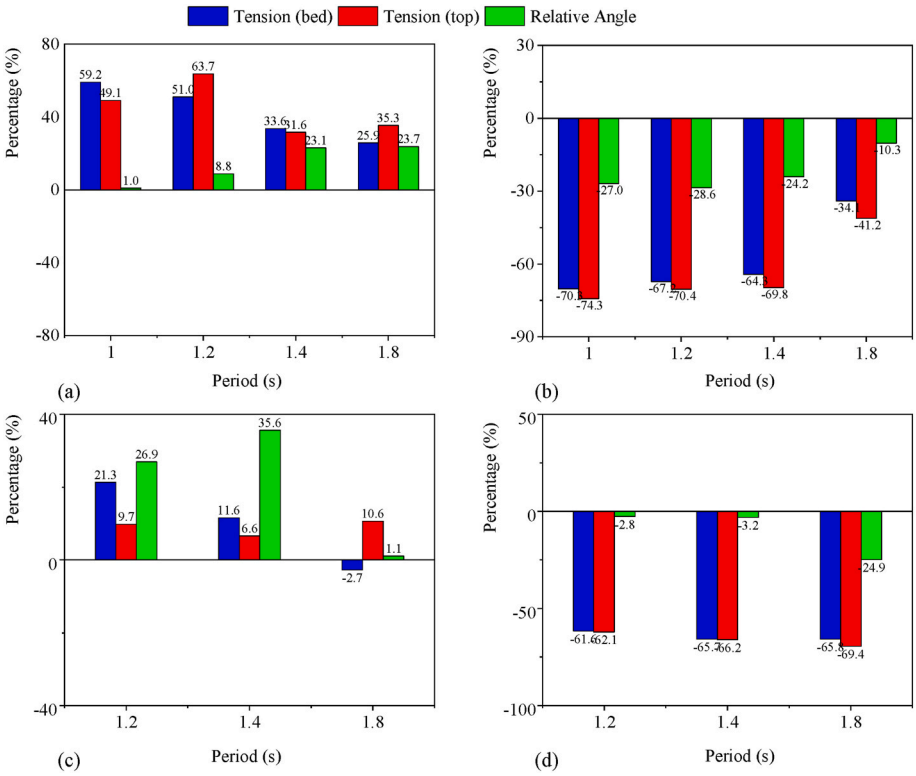

Fig. 22. M4hydro model errors for mooring forces and relative angle for cases in Table 3: (a) mean tension and rms relative angle for small H_s, (b) peak values for small H_s, (c) mean tension and rms relative angle for large H_s, (d) peak values large H_s.

Table 4
Scatter diagram peak fairlead force (kN) with % occurrence.

H_s (*m*)	T_e (s)				
	4	6	8	10	12
6.5	0	0	3125 (0.1%)	0	0
5.5	0	0	2625 (0.7%)	2125 (0.3%)	0
4.5	0	3125 (0.1%)	2375 (1.3%)	1875 (0.3%)	0
3.5	0	2625 (3.2%)	2000 (3.4%)	1375 (0.3%)	0

Table 5
Scatter diagram mean fairlead force (kN) with % occurrence.

H_s (*m*)	T_e (s)				
	4	6	8	10	12
6.5	0	0	500 (0.1%)	0	0
5.5	0	0	375 (0.7%)	190 (0.3%)	0
4.5	0	325 (0.1%)	225 (1.3%)	100 (0.3%)	0
3.5	0	250 (3.2%)	125 (3.4%)	75 (0.3%)	0

focussed waves was found to be linear (Santo et al., 2017), the underestimation of rms by Orcaflex and overestimation by M4hydro code appears inconsistent. The underestimation of peak response with a linear model is consistent with steep wave effects not being taken into account. Orcaflex underestimates mooring forces except for the peak hawser forces, which can be considerably overestimated presumably due to the effect of high stiffness in the model. The underestimation of peak forces in the M4hydro model is probably due to steep wave effects not represented in a linear model.

The good linear prediction of response by M4hydro for small (operational) waves with no drag coefficient (Stansby et al., 2017; Carpintero Moreno and Stansby, 2019) has been empirically extended to large waves with the incorporation of a drag coefficient. A value of unity is a compromise giving overestimates of rms and underestimates of peak values. The general underestimate by Orcaflex without any drag effect is unexplained. The mooring forces are more complex and mean values are small but important. The general underestimation by Orcaflex is again unexplained although the overestimation of hawser tension is probably due to the modelling of a large stiffness cable. The simple M4hydro model with a drag coefficient tuned for large waves gives mean forces within 21% and peak forces underestimate up to 70%, although less error than Orcaflex. Non-zero difference and sum frequencies are not included, and their influence is not apparent in the experimental force spectra.

Efficient hydrodynamic modelling is essential for design and work is ongoing to include nonlinear Froude-Krylov forces defined by nonlinear irregular waves, including breaking, and hydrostatic stiffness effects defined by the submerged body configuration (Li and Stansby, 2022). The submerged volume may also be used to modify the added mass and damping of the radiation forces.

7. Conclusions

Wave basin experiments using JONSWAP spectra for a representative range of peak periods have shown how peak and mean mooring forces and rotational response on a multi-float hinged attenuator-type WEC M4 with elastic mooring lines increase as wave height is increased. The mooring consists of an elastic cable anchored to the bed and attached to a single buoy and a further almost inelastic cable or hawser from the buoy to the bow float. Two elastic stiffnesses were used with the more elastic cable giving smaller mooring forces. The snap loads in large waves were up to a factor of 6 less than previous measurements with inelastic cables. Floats were overtopped (dunked) in very steep, occasionally breaking waves, limiting response and effectively providing a passive end stop, the largest peak relative angle being just less than 40° for the more elastic cable. The magnitude of bed tension is generally greater than the fairlead force with similar spectra, which are quite

complex with peaks at the mid/stern pitch natural frequency, the sum of this frequency and the bow/mid natural frequency, the wave frequency and the buoy heave frequency to a lesser degree. In contrast, relative pitch angle spectra show a prominent peak at the bow/mid pitch natural frequency, except for the smallest period with frequency and peak close to the mid/stern pitch frequency, and the wave frequency to a lesser degree. Although the hydrodynamics and float responses are highly nonlinear, a linear diffraction-radiation model M4hydro gives approximate predictions of rms relative angles, incorporating an empirical drag coefficient for all dissipative effects, in this case, tuned for extreme waves. The mean forces are overestimated, but the peak or snap mooring loads are underestimated markedly, as steep wave effects are absent in a linear model, and the mooring model is assumed quasi-steady. The Orcaflex model gave less close agreement generally underestimating apart from overestimating the peak hawser force, modelled dynamically. Considering the scatter diagram for a representative UK wave energy site, Wavehub, requiring a scale of 50x that in the laboratory, the peak fairlead force for a 1:1000 annual hourly sea state is about 312 tonnes with a mean of 50 tonnes. With a total mass for the 6-float system with a ballast of nearly 7000 tonnes, this peak force is only 4.5%. Elastic cables thus appear suitable for such systems, but general optimization should be undertaken. That articulated multi-float systems with elastic moorings result in such small loads suggests the potential for floating offshore platforms more generally, beyond wave energy conversion.

Author credit

Peter Stansby: Conceptualisation, Methodology, Software, Validation, Formal analysis, Investigation, Resources, Writing - Original Draft Preparation, Writing - Review & Editing, Visualisation, Supervision, Project administration, Funding acquisition. **Sam Draycott**: Methodology, Software, Validation, Formal analysis, Writing - Original Draft Preparation, Writing - Review & Editing, Visualisation, Supervision, Funding acquisition. **Gangqiang Li**: Methodology, Software, Formal analysis, Investigation, Writing - Review & Editing, Visualisation. **Chenyu Zhao**: Software (Orcaflex), validation. **Efrain Carpintero Moreno**: Formal analysis, Visualization. **Ajit Pillai**: Methodology, Supervision, Writing - Review & Editing. **Lars Johanning**: Methodology, Supervision, Writing - Review & Editing.

Declaration of competing interest

The authors declare that they have no known competing financial interests or personal relationships that could have appeared to influence the work reported in this paper.

Data availability

Data will be made available on request.

Acknowledgements

Support for Lir ocean basin access through the EU Marinet2 programme for this project M4moor (reference number 5031) and for funding through the EPSRC MoorWEC grant EP/V039946/1 is gratefully acknowledged. The electronics technician Robert Brown gave excellent support.

References

Carpintero Moreno, E., Stansby, P., 2019. The 6-float wave energy converter M4: ocean basin tests giving capture width, response and energy yield for several sites. Renew. Sustain. Energy Rev. 104, 307–318.

Cummins, W., Iiuhl, W., Uinm, A., 1962. The Impulse Response Function and Ship Motions. David Taylor Model Basin (DTNSRDC).

Davidson, J., Ringwood, J.V., 2017. Mathematical modelling of mooring systems for wave energy converters-A review. Energies 10 (5), 666.

Greenpromise, 2021. https://www.amazon.co.uk/gp/product/B073XJS7Z6.

Gu, H., Stansby, P., Stallard, T., Carpintero Moreno, E., 2018. Drag, added mass and radiation damping of oscillating vertical cylindrical bodies in heave and surge in still water. J. Fluid Struct. 82, 343–356.

Gunn, K., Stock-Williams, C., 2012. Quantifying the global wave power resource. Renew. Energy 44, 296–304.

Hann, M., Greaves, D., Raby, A., Howey, B., 2018. Use of constrained focused waves to measure extreme loading of a taut moored floating wave energy converter. Ocean Eng. 148, 33–42.

Hasselmann, K., et al., 1973. Measurements of wind-wave growth and swell decay during the joint North sea wave project (JONSWAP). Deuts. Hydrograph. Z. Reihe A 8 (12).

Johanning, L., Smith, G., 2009. Consideration of the cost implications for mooring MEC devices. Deliverable D7, 3. http://www.equimar.org/equimar-project-deliverables.html.

Lee, C., Newman, J., 2013. WAMIT User Manual, Version 7.0. WAMIT Inc, Chestnut Hill, Massachusetts.

to appear Li, G., Stansby, P., 2022. A general computing platform for offshore renewable energy systems (OREGEN). In: 5th Int. Conf. On Renewable Energies Offshore.

Liao, Z., Stansby, P., Li, G., Moreno, E.C., 2021. High-capacity wave energy conversion by multi-float, multi-PTO, control and prediction: generalized state-space modelling with linear optimal control and arbitrary headings. IEEE Trans. Sustain. Energy 12 (4), 2123–2131.

Mei, C.C., 1989. The Applied Dynamics of Ocean Surface Waves. World scientific.

Orcaflex, 2012. Manual Online at http://www. orcina. com/SoftwareProducts/OrcaFlex/Documentation. OrcaFlex. pdf.

Paduano, B., Giorgi, G., Gomes, R.P.F., Pasta, E., Henriques, J.C.C., Gato, L.M.C., Mattiazzo, G., 2020. Experimental validation and comparison of numerical models for the mooring system of a floating wave energy converter. J. Mar. Sci. Eng. 8 (8), 565.

Santo, H., Taylor, P.H., Carpintero Moreno, E., Stansby, P., Eatock Taylor, R., Sun, L., Zang, J., 2017. Extreme motion and response statistics for survival of the three-float wave energy converter M4 in intermediate water depth. J. Fluid Mech. 813, 175–204.

Stallard, T.J., Weller, S.D., Stansby, P.K., 2009. Limiting heave response of a wave energy device by draft adjustment with upper surface immersion. Appl. Ocean Res. 31 (4), 282–289.

Stansby, P., Carpintero Moreno, E., Stallard, T., Maggi, A., 2015. Three-float broad-band resonant line absorber with surge for wave energy conversion. Renew. Energy 78, 132–140.

Stansby, P., Carpintero Moreno, E., 2020a. Hydrodynamics of the multi-float wave energy converter M4 with slack moorings: time domain linear diffraction-radiation modelling with mean force and experimental comparison. Appl. Ocean Res. 97 (April), 102070.

Stansby, P., Carpintero Moreno, E., 2020b. Study of snap loads for idealized mooring configurations with a buoy, inextensible and elastic cable combinations for the multi-float M4 wave energy converter. Water 12 (10), 2818.

Stansby, P., Carpintero Moreno, E., Stallard, T., 2017. Large capacity multi-float configurations for the wave energy converter M4 using a time-domain linear diffraction model. Appl. Ocean Res. 68 (October), 53–64.

Thomsen, J.B., Ferri, F., Kofoed, J.P., Black, K., 2018. Cost optimization of mooring solutions for large floating wave energy converters. Energies 11 (1), 159.

Weller, S.D., Johanning, L., Davies, P., Banfield, S.J., 2015. Synthetic mooring ropes for marine renewable energy applications. Renew. Energy 83 (November), 1268–1278.

Xu, K., Larsen, K., Shao, Y., Zhang, M., Gao, Z., Moan, T., 2021. Design and comparative analysis of alternative mooring systems for floating wind turbines in shallow water with emphasis on ultimate limit state design. Ocean Eng., 108377

To appear Zhao, C., Li, G., Stansby, P., Johanning, L., 2022. Comparison of the full dynamic mooring simulation and wave basin test of a multi-float WEC. In: 5th Int. Conf. On Renewable Energies Offshore.

Pillai, A.C., Thies, P.R., Johanning, L., 2018. Development of a Multi-Objective Genetic Algorithm for the Design of Offshore Renewable Energy Systems. In: Schumacher, A., Vietor, T., Fiebig, S., Bletzinger, KU, Maute, K. (Eds.), Advances in Structural and Multidisciplinary Optimization. https://doi.org/10.1007/978-3-319-67988-4_149. WCSMO 2017., 12. Springer, Cham.